

Article

Effect of Aging Temperature on Precipitates Evolution and Mechanical Properties of GH4169 Superalloy

Anqi Liu ^{1,2}, Fei Zhao ^{1,2,*}, Wensen Huang ^{1,2}, Yuanbiao Tan ^{1,2} , Yonghai Ren ³, Longxiang Wang ³ and Fahong Xu ⁴

- ¹ College of Materials and Metallurgy, Guizhou University, Guiyang 550025, China; liuanqi9797@163.com (A.L.); huangws89@163.com (W.H.); ybtan1@gzu.edu.cn (Y.T.)
² Key Laboratory for Materials Structure and Strength of Guizhou Province, Guiyang 550025, China
³ Guiyang Anda Aerospace Material Engineering Co., Ltd., Guiyang 550009, China; yonghairan@163.com (Y.R.); sonilgtcl@163.com (L.W.)
⁴ Guizhou Special Equipment Inspection and Testing Institute, Guiyang 550016, China; xfh598@163.com
* Correspondence: fzhao@gzu.edu.cn

Abstract: GH4169 is primarily strengthened through precipitation, with heat treatment serving as a crucial method for regulating the precipitates of the alloy. However, the impact of aging temperature on the microstructure and properties of GH4169 has not been thoroughly studied, hindering effective regulation of its microstructure and properties. This study systematically investigated the effects of aging temperature on the evolution of precipitates and mechanical properties of GH4169 alloy using various techniques such as OM, SEM, XRD and TEM. The results indicate that raising the aging temperature leads to an increase in the sizes of both the γ'' and γ' phases in the alloy, as well as promoting the precipitation of δ phase at grain boundaries. Notably, the increase in γ'' phase size enhances the strength of the alloy, while the presence of δ phase is detrimental to its strength but greatly enhances its elongation. The yield strength of the alloy aged at 750 °C exhibits the highest yield strength, with values of 1135 MPa and 1050 MPa at room temperature and elevated temperature, respectively. As the aging temperature increases, the Portevin-Le Châtelier (PLC) effect during elevated temperature tensile tests at 650 °C gradually weakens. The PLC effect disappears almost completely when the aging temperature reaches 780 °C.

Keywords: GH4169 alloy; aging temperature; γ'' phase; δ phase; mechanical properties



Citation: Liu, A.; Zhao, F.; Huang, W.; Tan, Y.; Ren, Y.; Wang, L.; Xu, F. Effect of Aging Temperature on Precipitates Evolution and Mechanical Properties of GH4169 Superalloy. *Crystals* **2023**, *13*, 964. <https://doi.org/10.3390/cryst13060964>

Academic Editors: Daniel Medyński, Grzegorz Lesiuk and Anna Burduk

Received: 24 May 2023
Revised: 12 June 2023
Accepted: 15 June 2023
Published: 17 June 2023



Copyright: © 2023 by the authors. Licensee MDPI, Basel, Switzerland. This article is an open access article distributed under the terms and conditions of the Creative Commons Attribution (CC BY) license (<https://creativecommons.org/licenses/by/4.0/>).

1. Introduction

GH4169 (Inconel718) is a highly utilized superalloy in various industries such as aerospace and petroleum due to its exceptional mechanical properties [1,2]. The key contributors to its excellent mechanical properties are the precipitates within the matrix, which include the γ'' (Ni_3Nb) phase, γ' ($\text{Ni}_3(\text{Al,Ti})$) phase and δ (Ni_3Nb) phase. The γ'' phase is the main strengthening phase with an ordered body-centered tetragonal DO_{22} crystal structure, and the precipitation temperature range is 595–870 °C [3]. The strengthening effect of γ' phase is less than γ'' phase, which is a secondary strengthening phase with a face-centered cubic L1_2 crystal structure. The precipitation temperature range is 593–816 °C [4]. The formation of the γ'' phase and γ' phase occurs during the two-stage aging process. In the conventional double aging process (720 °C/8 h + 620 °C/8 h), the purpose of aging at 720 °C is to mainly precipitate the γ'' phase, while aging at 620 °C is mainly to precipitate the γ' phase [5,6]. The δ phase is typically incoherently precipitated with the matrix, with a precipitation temperature range of 750–1020 °C [7]. It is worth noting that the γ'' phase is a metastable phase in GH4169 alloy. The γ'' phase transforms into the δ phase when the alloy is subjected to long-term aging or high temperatures, thereby reducing the strengthening effect of the alloy. This limits the maximum temperature at which the alloy can be used to less than 650 °C [8,9].

The precipitation behavior of the γ'' and γ' phases in GH4169 alloy is affected by temperature, with their nucleation and growth closely tied to aging temperatures. Altering the aging temperature can impact precipitate precipitation, which in turn affects the mechanical properties of the alloy. Rafiei et al. [10] discovered that the precipitation kinetics of the γ'' phase is highly dependent on aging temperature, with the maximum precipitation rate occurring at 780 °C. But Drexler et al. [11] discovered that the temperature at which precipitation occurs most rapidly is 750 °C. In a study by Fisk et al. [12], it was found that the aging temperature has a significant impact on the hardness of Inconel718. By analyzing the change in hardness, they determined that the sample aged at 760 °C for 8 h exhibited the highest level of hardness. The γ'' and γ' phases are coherent with the matrix and can be cut by dislocations, resulting in a strengthening effect. The increase in strength caused by dislocation cutting the second phase is related to the size of the second phase. Qin et al. [13] found that when the volume fraction was similar, the strength displayed a rising trend with the increase of γ'' phase size. A similar phenomenon was reported in the study by Ran et al. [14]. They quantitatively calculated the contribution of the precipitated phase to the strength and found that the strength change is sensitive to the size of the γ'' phase. They also observed that the strengthening effect of large size γ'' phase is more significant. The precipitation of the δ phase in GH4169 alloy can enhance its plasticity [15,16]. However, since the δ phase has the same chemical composition as the γ'' phase, excessive precipitation of the former can result in a decrease in the formation element Nb of the latter, ultimately leading to a reduction in strength [17].

In summary, the precipitation behavior of the γ'' and γ' phases in the alloy is significantly influenced by the aging temperature. Additionally, a competitive relationship exists between the γ'' and δ phases. The γ'' phase positively impacts the strength of the alloy, while the acquisition of the δ phase can improve its plasticity. Heat treatment is a crucial method for regulating the precipitates in GH4169 superalloy. However, current research on the precipitation behavior of precipitates through heat treatment remains insufficient. This study involved the preparation of three distinct GH4169 samples, each with a different heat treatment scheme. The impact of aging temperature on the second phase of GH4169 alloy was investigated using various techniques including OM, XRD, SEM and TEM. The study aimed to establish the relationship between the microstructure characteristics and mechanical properties of the alloy by examining the effects of the second phase characteristics on the tensile properties of the alloy at both room and elevated temperatures.

2. Materials and Methods

The material used in this study was commercial GH4169 superalloy, whose chemical compositions is shown in Table 1. Before undergoing the aging treatment, the samples underwent a solution treatment at a temperature of 1030 °C for a duration of 1 h to dissolve any precipitates present in the matrix. The microstructure after solution treatment is shown in Figure 1, which is composed of equiaxed grains and a small amount of carbides, and the average grain size is 81 μm . The samples after solid solution were treated with different heat treatments: (1) isothermal at 720 °C for 8 h, followed by furnace cooling to 620 °C at the rate of 50 °C/h, isothermal at 620 °C for 8 h, and then air cooling, recorded as A720; (2) isothermal at 750 °C for 8 h, followed by furnace cooling to 620 °C at the rate of 50 °C/h, isothermal at 620 °C for 8 h, and then air cooling, recorded as A750; (3) isothermal at 780 °C for 8 h, followed by furnace cooling to 620 °C at the rate of 50 °C/h, isothermal at 620 °C for 8 h, and then air cooling, recorded as A780. Aging treatments were carried out in a box-type heat treatment furnace with air as the medium.

Table 1. Chemical composition of GH4169 alloy.

| Element | Ni | Si | Mn | C | Cr | Mo | Al | Ti | Nb | Fe |
|---------|-------|-------|------|-------|-------|-------|-------|-------|-------|-----|
| Wt.% | 51.72 | 0.048 | 0.02 | 0.028 | 18.86 | 3.007 | 0.519 | 0.947 | 5.212 | Bal |

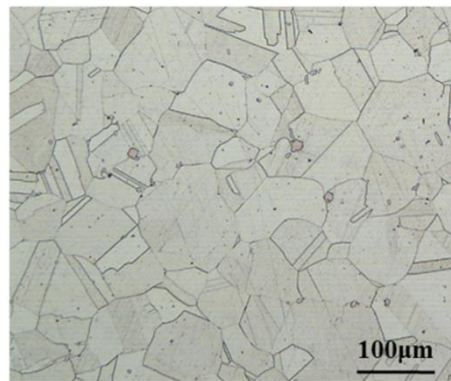


Figure 1. Microstructure of GH4169 alloy after solution treatment.

The aged samples were cut into tensile samples of the size indicated in Figure 2. Among them, the thickness of the tensile sample at room temperature was 2 mm. Prior to testing, the tensile samples were smoothed with sandpaper to eliminate cutting marks and oxide layers. The MTS 810 electro-hydraulic servo testing machine was used to conduct the tensile tests at a rate of 1 mm/min. To eliminate the influence of temperature gradient during elevated temperature tensile test (650 °C), the test was carried out after 20 min of heat preservation. The samples were cooled to room temperature in the air after fracture. In order to observe the fracture morphology, samples were cut along the direction perpendicular to the tensile direction near the fracture, and SEM observation was performed after ultrasonic cleaning with alcohol.

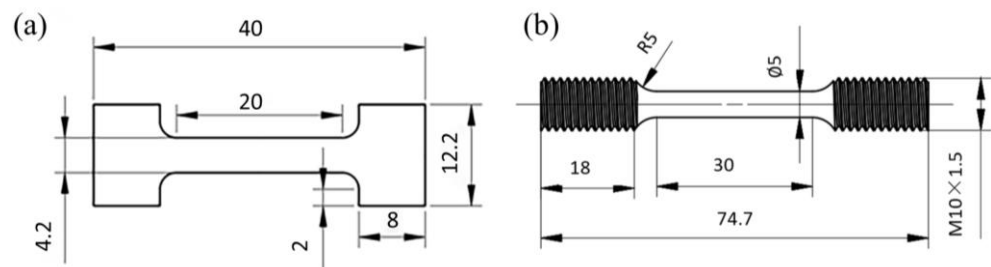


Figure 2. Schematic diagram with dimensions (in mm) of tensile samples: (a) room temperature tensile specimen; (b) elevated temperature tensile specimen.

OM, SEM and TEM were used to characterize the microstructure of the samples. Before OM and SEM observation, the samples need to be polished first and then corroded with 2.5 g CuCl_2 + 50 mL HCl + 50 mL $\text{CH}_3\text{CH}_2\text{OH}$ solution at room temperature. TEM samples were sampled on the samples after aging treatment. The samples were mechanically ground to about 50 μm , and the samples were punched into small round pieces with a diameter of 3 mm by a sample puncher. Then, electrolytic polishing was carried out. The precipitates of the samples were characterized by FEI F200X TEM, and the test voltage was 200 kV. The phase characteristics were determined by XRD using $\text{Cu K}\alpha$ radiation in a range for 2θ of 20–100° at a scanning speed of 2°/min. The size and content of precipitates in SEM and TEM images were analyzed by Image-Pro Plus 6.0 software. Five pictures of each sample were selected for statistics.

3. Results and Discussions

3.1. Effect of Aging Temperature on Mechanical Properties

3.1.1. Microhardness

Table 2 shows the microhardness of the alloys that were aged at three different temperatures. The results indicate that the hardness of A720, A750 and A780 alloys are 418.9 HV, 471.8 HV and 453.5 HV, respectively. As the aging temperature increases, the hardness of

the alloy initially increases and then decreases. Additionally, the hardness of the A750 and A780 samples is greater than that of the A720 samples.

Table 2. Microhardness of samples at different aging temperatures.

| Samples | A720 | A750 | A780 |
|-------------|-------|-------|-------|
| Hardness/Hv | 418.9 | 471.8 | 453.5 |

3.1.2. Tensile Properties at Room Temperature

Figure 3 shows the engineering stress–strain curves and specific mechanical properties data histogram for the three heat-treated alloys at room temperature. The graph in Figure 3b indicates that as the aging temperature increases, the yield strength (YS) and ultimate tensile strength (UTS) of the alloy experience a significant increase initially, followed by a slight decrease. The yield strength and ultimate tensile strength of the A750 alloy are the highest, 1135 MPa and 1345 MPa, respectively, which are 13.5% and 8.9% higher than that of the A720 alloy. Furthermore, it can be found that the elongation (EL) of A750 and A780 alloys is not much different, but it is significantly lower than that of the A720 alloy. The A750 alloy has the highest yield strength and ultimate tensile strength, measuring at 1135 MPa and 1345 MPa, respectively. These values are 13.5% and 8.9% higher than those of the A720 alloy.

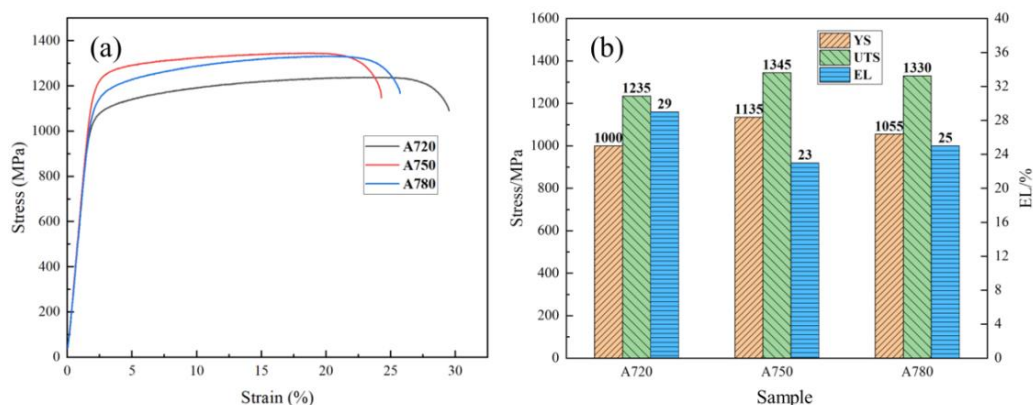


Figure 3. Tensile test at room temperature of specimens at different aging temperatures: (a) stress–strain curves; (b) strength and ductility values.

3.1.3. Tensile Properties at Elevated Temperature

Figure 4a shows the hot tensile stress–strain curves of the three aged samples at 650 °C. The specific tensile strength data are presented in Figure 4b, which shows that the yield strength of the alloy increases initially and then decreases with the increase in aging temperature. The yield strength of A750 and A780 alloys is considerably higher than that of the A720 alloy. The yield strength of the A750 alloy is 1050 MPa, which represents an 11% increase compared to that of the A720 alloy. Both the A720 and A780 alloys have good plasticity of 26%, which is obviously better than A750 alloy. Additionally, the ultimate tensile strength of the alloys increases with the aging temperature, as shown in Figure 4b. The ultimate tensile strengths of A720, A750 and A780 alloys are 1105 MPa, 1185 MPa and 1210 MPa, respectively. During high temperature tensile tests, both A720 and A750 alloys exhibit typical dynamic strain aging phenomenon, except for the A780 alloy, as illustrated in Figure 4a.

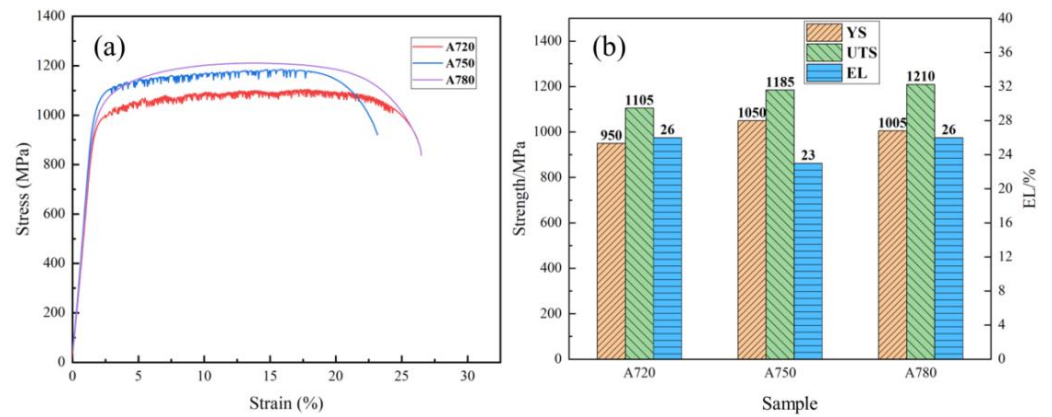


Figure 4. Tensile test at elevated temperature of specimens at different aging temperatures: (a) stress–strain curves; (b) strength and ductility values.

3.2. Relationship between Microstructure Evolution and Mechanical Properties

Figure 5 shows the optical microscope images of GH4169 alloy following three aging processes. The images reveal that the grains remain equiaxed, with a small presence of twins and bulk precipitates. The bulk precipitate was analyzed using energy dispersive spectroscopy (EDS), with the result presented in Figure 5d. The EDS analysis indicates that these bulk precipitates are carbides such as NbC or TiC. The grain size of the aged alloy was measured using the transversal method in Image-Pro Plus 6.0 software. The average grain sizes of A720, A750 and A780 alloys are 84 μm , 86 μm and 87 μm , respectively. Upon comparing the metallographic image of the solid solution alloy shown in Figure 1, it was observed that the aging temperature had no effect on the grain size of the alloy.

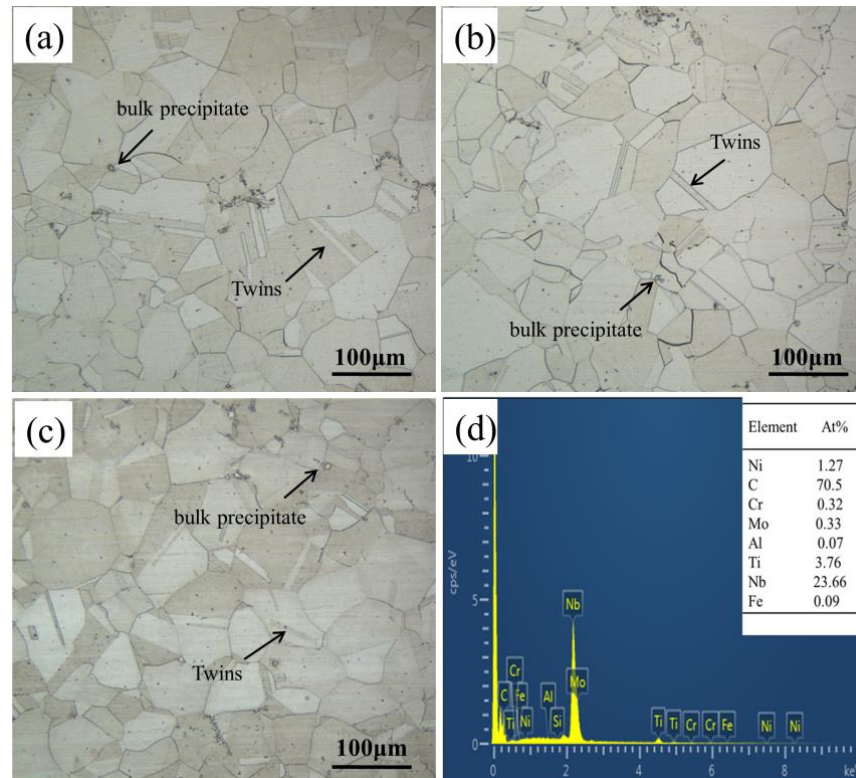


Figure 5. Microstructure of GH4169 treated at different aging temperatures: (a) A720; (b) A750; (c) A780; (d) EDS analysis of bulk precipitates.

Figure 6 shows the results of XRD phase analysis of the three heat-treated alloys. From the diagram, there is no obvious difference between the diffraction patterns of the three alloys. The diffraction peaks with higher diffraction intensity correspond to γ (111), γ (200) and γ (220), respectively. No diffraction peak of δ phase was observed in Figure 6, which may be due to the absence of δ phase precipitation or the low content of δ phase in GH4169 alloy after heat treatment. In addition, the absence of diffraction peaks of γ'' and γ' phases in the diagram can be attributed to their coherence with the γ matrix. As a result, the peaks of γ' (111) and γ (111) coincide; γ' (200) and γ'' (200) peaks coincide with the γ (200) peak; and γ' (220) and γ'' (220) peaks coincide with the γ (220) peak.

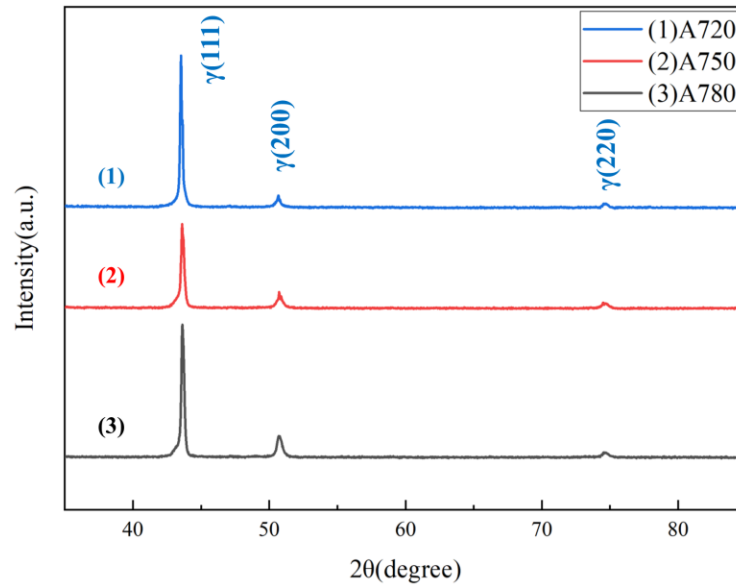


Figure 6. XRD patterns of three heat-treated samples.

The results from Figures 3 and 4 indicate that the yield strength and ultimate tensile strength of the A750 alloy and the A780 alloy are significantly improved compared with the A720 alloy. In general, the main strengthening mechanisms for nickel-based superalloys include solution strengthening, precipitation strengthening, dislocation strengthening and grain boundary strengthening [18,19]. The contribution of solution strengthening to strength was consistent across the three aged samples due to the presence of the same alloying elements in the matrix. The grain size of the alloy was not affected by the aging temperature, as evidenced by Figure 5, leading to similar grain boundary strengthening effects. Additionally, the XRD pattern in Figure 6 showed similar peak widths across all three aging treatment samples. This indicates that the lattice strain (ϵ) is similar. According to the calculation formula of dislocation density $\rho = 16.1\epsilon^2/b^2$ (ρ is dislocation density, and b is the Burgers vector of GH4169 alloy) [20], there is no significant difference in dislocation density among the three aged samples, which leads to the similar contribution of dislocation strengthening to strength. Therefore, the strength difference of the three aged samples mainly comes from precipitation strengthening.

The TEM images of the alloy after three aging processes are presented in Figure 7. The bright field images of the alloy are shown in Figure 7a,d,g, accompanied by their corresponding selected area electron diffraction patterns in Figure 7b,e,h. The diffraction patterns of the aged alloys exhibit similar characteristics, consisting of distinct matrix diffraction spots and faint precipitates diffraction spots. The identified weak diffraction spots are characteristic of γ'' and γ' superlattice diffraction, indicating that the fine precipitates dispersed in the matrix are γ'' and γ' phases. The γ'' and γ' phases cannot be distinguished and counted in the bright field image due to the lack of contrast between the precipitates and the matrix. To determine the size and volume fraction of the γ'' and γ' phases, dark field images analysis with (002) γ'' was performed, as illustrated in Figure 7c,f,i. It can be

seen from the dark field images that the size of the precipitates increases significantly with the increase in the aging temperature, which is consistent with the phenomenon observed by SEM.

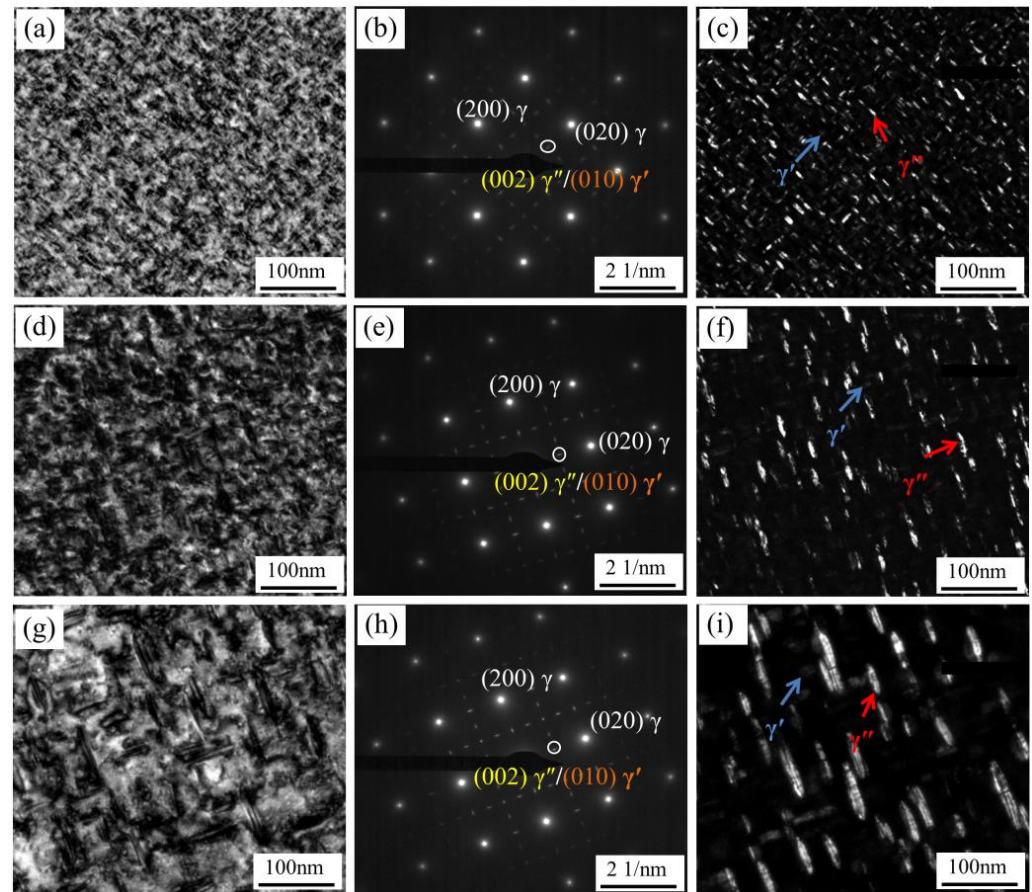


Figure 7. TEM image of γ'' and γ' phases: (a), (d) and (g) are the bright field images of samples A720, A750 and A780, respectively; (b), (e) and (h) are the selected electron diffraction patterns of γ'' and γ' in A720, A750 and A780 samples, respectively; (c,f,i) are the dark field images of A720, A750 and A780 samples made by $(002) \gamma''$ diffraction spots.

The size of about 400 precipitates in the dark field image of each aged sample was measured, and the volume fraction was counted. For the disk-like γ'' phase, the dimensions of its long axis and short axis are measured respectively, and for the spherical γ' phase, the diameter is measured. The results are shown in Table 3. As the aging temperature increases, the growth of γ'' and γ' phases becomes more apparent, with γ'' growing particularly along the long axis. The size of the γ'' phase along the long axis increases from 13.6 nm in the A720 alloy to 47 nm in the A780 alloy, while the diameter of the γ' phase increases from 7.1 nm in the A720 alloy to 17.5 nm in the A780 alloy. The volume fraction of the second phases does not change significantly.

Table 3. Size and volume fraction statistics of γ'' and γ' phases.

| Specimen | γ'' | | | γ' | | |
|----------|-----------------------|------------------------|-------|-------------------|--------------|-------------------|
| | Mean Long Axis (R)/nm | Mean Short Axis (H)/nm | H/R | Volume Fraction/% | Diameter /nm | Volume Fraction/% |
| A720 | 13.6 | 4 | 0.294 | 13.4 | 7.1 | 3.4 |
| A750 | 30 | 8.5 | 0.283 | 12.4 | 13 | 2.7 |
| A780 | 47 | 9.6 | 0.204 | 12.3 | 17.5 | 2.4 |

In order to understand the interface relationship between the γ'' phase and the matrix in different aged alloys, high-resolution transmission electron microscopy (HRTEM) and inverse fast Fourier transform (IFFT) observations were carried out. The results are shown in Figure 8. Based on the IFFT diagrams presented in Figure 8d–f, it is evident that the γ'' phases in the A720, A750 and A780 samples exhibit a strong coherence with the γ matrix interface, indicating a well-maintained coherent relationship between γ'' and the matrix. Slama et al. [21] believed that γ'' will lose the coherent relationship when the long axis size of γ'' is larger than 120 nm, while Devaux et al. [22] believed that the critical size is 95 nm. Combined with the data in Table 2, it can be seen that the size of γ'' obtained in this study is significantly smaller than the critical size reported in the literatures.

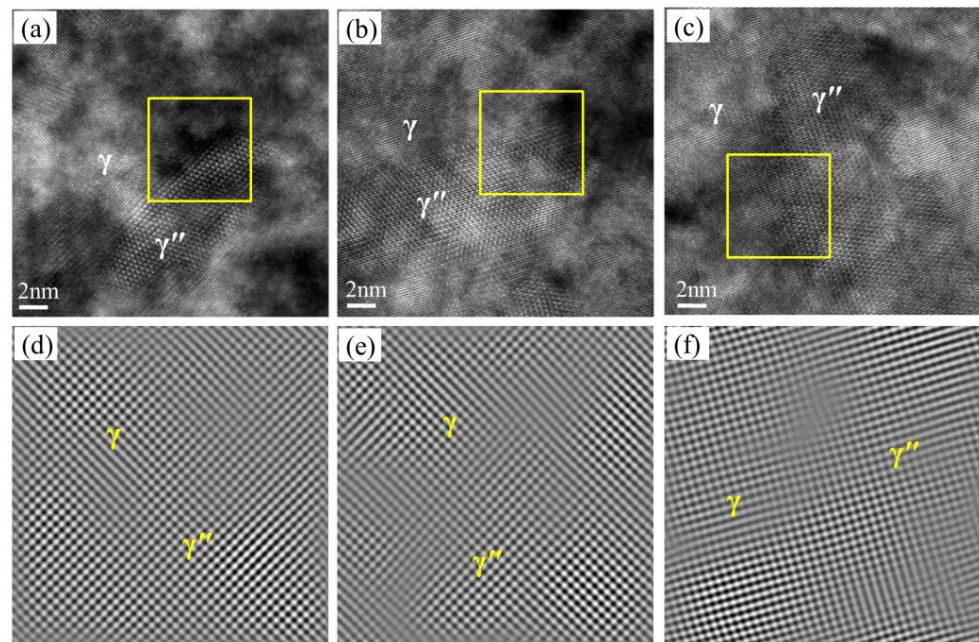


Figure 8. Interface relationship between γ'' phase and the matrix: (a–c) are HRTEM images of γ'' in A720, A750 and A780 samples, respectively; (d–f) are the IFFT images in the yellow box.

The strength of GH4169 alloy is primarily derived from the γ'' phase, which is caused by the coherent strain resulting from the lattice mismatch between the γ'' phase and the matrix. In the case of ellipsoidal precipitates with tetragonal distortion perpendicular to the habit plane, the relationship between coherent strain (ε^c) and stress-free strain (ε^T) can be expressed as [23]:

$$\varepsilon^c = \left[1 - \frac{(1 - 2\nu) \alpha}{2(1 - \nu) R} \right] \varepsilon^T \quad (1)$$

where $\alpha = 4h/3$ is the thickness of ellipsoidal particles with long axis R and short axis h ; ν is Poisson's ratio ($\nu = 1/3$), $\varepsilon^T = 0.0286$. It can be seen that the ratio of the short axis to the long axis of the γ'' phase can result in a greater coherent strain, which is consistent with previous research by Lu et al. [24]. The γ'' phases in the three aged alloys in this study maintain a good coherent relationship with the matrix. As the aging temperature increased, the increase of γ'' phase size was accompanied by the decrease of short axis and long axis ratio, which led to the increase in coherent strain. When the dislocation passed through the coherent strain zone, the ability to hinder the dislocation was enhanced, resulting in a greater strengthening effect.

In precipitation-strengthened nickel-based superalloys, the strengthening effect is primarily achieved by impeding dislocations through precipitates. The main mechanism for strengthening is through dislocation shearing or bypassing. Qin et al. [25] discovered that dislocation cut-through is the main mechanism for strengthening the GH4169 alloy when the long axis size of the γ'' phase is less than 90 nm. The long axis sizes of γ''

phases of the A720, A750 and A780 alloys in this study are 13.6 nm, 30 nm and 47 nm, respectively, which are all less than 90 nm. Therefore, the main strengthening mechanism can be considered as dislocation shearing. The increase of strength caused by the resistance of coherent precipitation to dislocation motion can be calculated by $\Delta\tau = \beta G \varepsilon^{\frac{3}{2}} (\frac{r}{b})^{\frac{1}{2}} f^{\frac{1}{2}}$ (β is a constant related to the dislocation type; G is the shear modulus; r and f are the size and content of the precipitated phases, respectively; and b is the Burgers vector of GH4169 alloy) [26]. It can be seen from the formula that the contribution of dislocation shearing to strength is closely related to the size of precipitates, and the larger size precipitation has a more prominent contribution to the strength improvement. In this paper, the volume fraction of γ'' phase obtained by the three aging processes is similar. The sizes of γ'' phases in the A750 and A780 alloys are significantly larger than that of the A720 alloy, which has a greater strengthening effect on the alloy. This corresponds to the increase in yield strength and ultimate tensile strength of the alloy in Figures 3 and 4 and the increase in hardness in Table 2.

The SEM images of the aged alloys are displayed in Figure 9. In the A720 alloy, the grain boundary appears to be relatively clean, as depicted in Figure 9a. The yellow arrow points out the absence of any noticeable precipitates after aging at 720 °C. On the other hand, in the A750 alloy, a few fine granular precipitates, measuring about 216 nm, emerge at the grain boundaries. EDS analysis indicates that the phase is a Nb-rich δ phase, as illustrated in Figure 9e. At an aging temperature of 780 °C, δ phases with a granular and short rod-like structure, measuring approximately 538 nm, precipitate at the grain boundary. These δ phases are larger than those found in A750 alloy. Additionally, needle-like δ phases with a length of about 1.5 μm appear within grains. It is worth noting that δ phase is not observed in the A720 alloy due to its precipitation temperature range of 750–1020 °C [27].

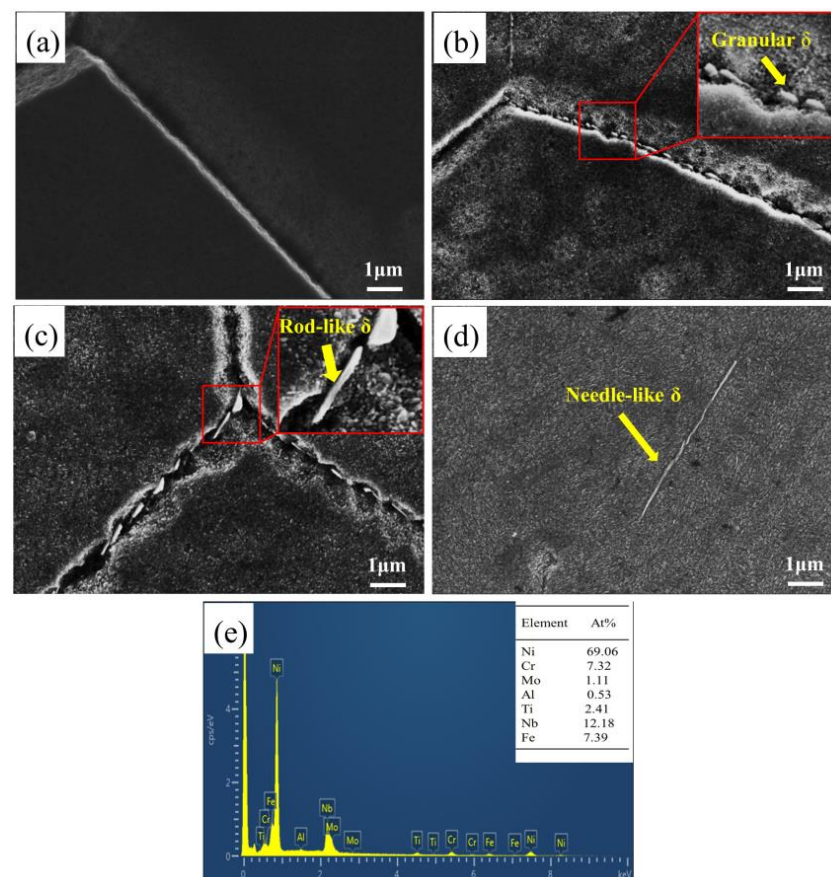


Figure 9. SEM images of δ phase of samples at different aging temperatures: (a) A720; (b) A750; (c) A780; (d) Intragranular δ phase of A780; (e) EDS analysis of grain boundary precipitates.

The strength of the A750 and A780 alloys is significantly improved compared with the A720 alloy due to the growth of the γ'' phase and the increase in dislocation hindrance. At the same time, the slip of dislocation is hindered, resulting in a decrease in plasticity. Upon analysis of the elevated temperature and room temperature tensile curves, it is evident that the sample aged at 750 °C has a higher yield strength than the sample aged at 780 °C, but the plasticity of the latter sample is better. This is due to the increase of the volume fraction of δ phase at the grain boundary, which is consistent with the results of Andersong et al. [28], who discovered that increasing the volume fraction of δ phases at grain boundaries can improve plasticity by reducing yield strength. This is because the formation of the δ phase will produce a γ'' phase missing zone around it, which has high plasticity and can alleviate stress concentration, thereby improving the plasticity of the alloy [29]. The increase in δ phase content also leads to a lower hardness of A780 alloy compared to A750 alloy, as shown in Table 2, which is consistent with the results of Rafiei et al. [10].

The fracture surfaces after room temperature tensile tests of the aged alloys are shown in Figure 10. There are a small amount of micro holes and a large number of dimples in the fracture surfaces of the alloys. In addition, a small number of microcracks were found in the fracture of the alloys, indicating that a large plastic deformation was experienced during the tensile tests. Figure 10b,c show the fracture surfaces of the A750 and A780 alloys at room temperature. The existence of dimples and holes can be observed, but the dimples are smaller and shallower than that of A720 alloy. In addition, cleavage faces were also found in the fracture surfaces of the A750 and A780 alloys, and the number of cleavage faces of A750 is more than that of the A780 alloy. According to the characteristics of fracture surfaces, the alloy aged at 720 °C has better plasticity, which just explains the law in Figure 3b.

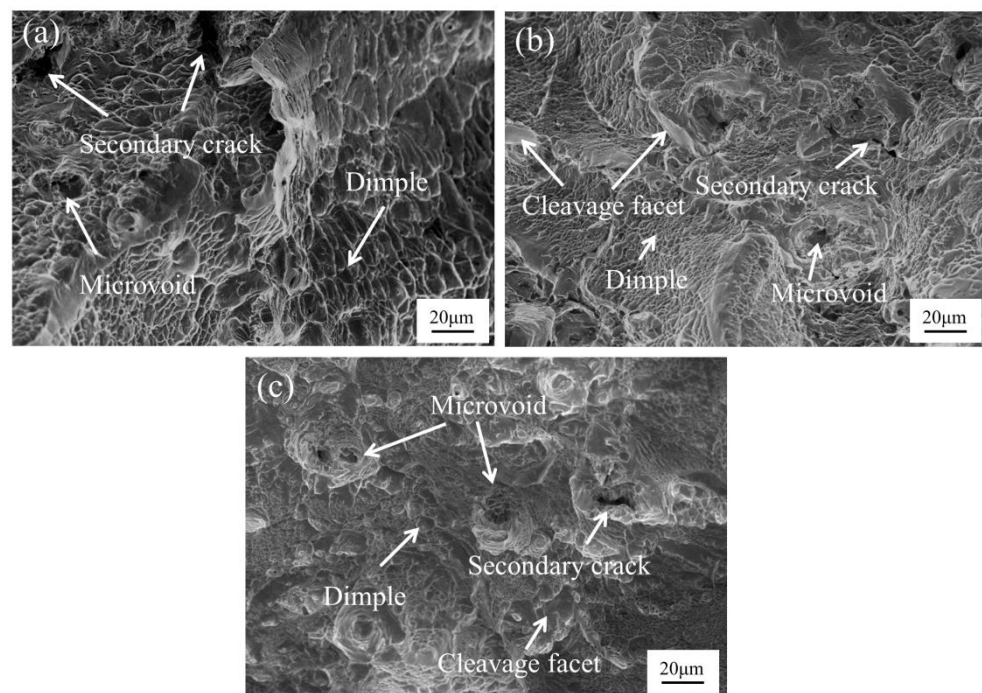


Figure 10. Fracture surfaces of tensile samples at room temperature: (a) A720; (b) A750; (c) A780.

The fractures of the tensile samples tested at 650 °C were analyzed by SEM, and the results are shown in Figure 11. Figure 11a,c are the morphologies of the fracture center of the A720 and A780 alloys after hot tensile, respectively, with a large number of dimples and a small amount of micro-pores. Figure 11b is the morphology of the central part of the fracture of the A750 alloy, which is significantly different from that of the A720 and A780 alloys. The dimple size in the fracture of the A750 alloy is significantly reduced, which corresponds to the deterioration of plasticity. In addition, there are inclusions at

the bottom of the pores in the fracture of the alloys. It can be judged by EDS analysis that these inclusions are NbC and TiC, as shown in Figure 11d. The plastic law presented by the fracture surfaces is consistent with the data in Figure 4b.

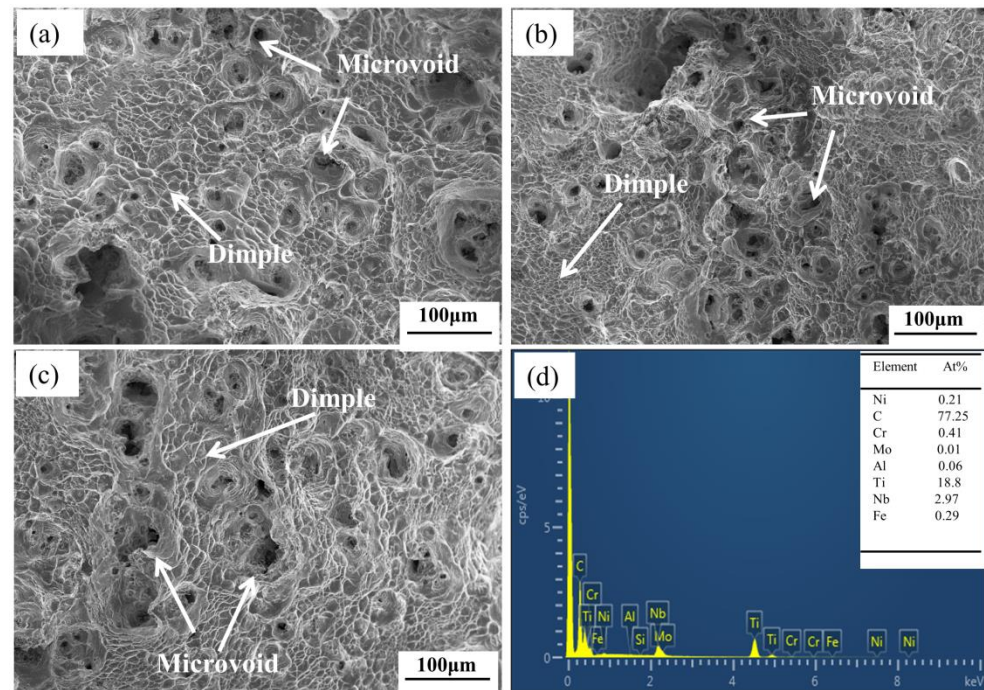


Figure 11. Fracture surfaces of tensile specimen at elevated temperature: (a) A720; (b) A750; (c) A780; (d) EDS analysis of inclusions at hole bottom.

The stress–strain curves in Figure 4a demonstrate the presence of PLC effects in alloys aged at 720 °C and 750 °C during elevated temperature tensile processes. As the aging temperature increases to 780 °C, the PLC effect becomes almost negligible. The PLC effect is generated by the interaction between moving dislocations and solute atoms, which is shown as a zigzag curve. The space of serration on the curve represents the time interval between the dislocation fixed by the atom and the dislocation separated from the atom. The space of serration on the curve gradually increases with the aging temperature. The size of the γ'' phase and the precipitation of δ phase significantly increase with the rise in aging temperature, as evidenced by Figures 7 and 9. The enlarged γ'' phase enhances the hindrance to dislocations, leading to a longer time for dislocations to pass through it. This results in an increase in the spacing of serration [30]. In addition, as the aging temperature increases, the formation and growth of γ'' phase and the precipitation of δ phase utilize a significant amount of solute atoms, leading to a reduction in solute atoms in the matrix. This decrease in solute atoms results in a longer time needed for dynamic strain aging, causing the serration space to increase [31]. In summary, the enhancement of the ability of γ'' phase to hinder dislocations and the reduction of solute atoms in the matrix lead to the disappearance of the PLC effect during the tensile process of the A780 alloy. The PLC effect will cause the surface roughness of the material and affect the mechanical properties of the alloy, which is not conducive to the processing and use of the alloy [32]. Increasing the aging temperature can effectively inhibit the PLC effect.

4. Conclusions

In this paper, the effects of aging temperatures (720 °C, 750 °C and 780 °C) on the precipitation behavior of γ'' , γ' and δ phases in GH4169 alloy were systematically studied, and the correlation between the characteristics of precipitates and the mechanical properties of the alloy at room temperature and elevated temperature was clarified. The following conclusions were drawn.

- (1) The size of the γ'' and γ' phases is significantly affected by the aging temperature, while the volume fraction remains relatively unchanged. As the aging temperature increases, the size of the γ'' and γ' phases increases greatly. Specifically, the size of the γ'' phase in the long axis direction increases from 13.6 nm in the A720 alloy to 47 nm in the A780 alloy. It is worth noting that the γ'' phase maintains a good coherent relationship with the matrix. Additionally, the diameter of the γ' phase increases from 7.1 nm in the A720 alloy to 17.5 nm in the A780 alloy.
- (2) The precipitation of the δ phase is promoted with an increase in aging temperature. When aged at 750 °C, granular δ phase precipitates at the grain boundary of the alloy. However, when aged at 780 °C, not only does granular δ phase form at the grain boundary, but needle-like δ phase is also formed within the grains. The size of δ phase formed at 780 °C is larger than that of the alloy aged at 750 °C.
- (3) The yield strength and ultimate tensile strength of alloys at room and elevated temperatures are increased due to the larger sizes of the γ'' phases, which create a greater coherent strain and strengthen the hindrance to dislocations. The alloy aged at 750 °C has the highest yield strength, measuring 1135 MPa at room temperature and 1050 MPa at elevated temperature. Compared to the alloy aged at 720 °C, the yield strength of the alloy increased by 13.5% and 10.5%, respectively. The δ phase is detrimental to the strength of the alloy, but it significantly increases the elongation of the alloy. When the aging temperature is 780 °C, the increase in the size of the γ'' phases enhances the hindrance of dislocations, and the precipitation of the γ'' and δ phases reduces the solute atoms in the matrix, both of which inhibit the PLC effect.

Author Contributions: Conceptualization, A.L., Y.R., L.W. and F.X.; investigation, A.L., Y.R., L.W. and F.X.; resources, A.L., L.W. and F.Z.; writing—original draft, A.L., W.H. and F.Z.; writing—review and editing, A.L., F.Z., W.H. and Y.T.; funding acquisition, F.Z., Y.R. and L.W.; supervision, A.L., W.H., F.Z. and Y.T. All authors have read and agreed to the published version of the manuscript.

Funding: This study was supported by Science and Technology granted by Guiyang city with Grant No. [2021]1-7 and the Guizhou science and technology project with Grant No. ZK [2022]023.

Data Availability Statement: Not applicable.

Conflicts of Interest: The authors declare no conflict of interest.

References

1. Tian, S.G.; Li, Z.R.; Zhao, Z.G.; Chen, L.Q.; Sun, W.R.; Liu, X.H. Influence of deformation level on microstructure and creep behavior of GH4169 alloy. *Mater. Sci. Eng. A* **2012**, *550*, 235–242.
2. Ran, R.; Wang, Y.; Zhang, Y.X.; Fang, F.; Wang, G.D. Microstructure, precipitates and mechanical properties of Inconel 718 alloy produced by two-stage cold rolling method. *Mater. Sci. Eng. A* **2020**, *793*, 139860. [[CrossRef](#)]
3. Zhu, J.; Yuan, W. Effect of pretreatment process on microstructure and mechanical properties in Inconel 718 alloy. *J. Alloys Compd.* **2023**, *939*, 168707. [[CrossRef](#)]
4. Deschamps, A.; Hutchinson, C.R. Precipitation kinetics in metallic alloys: Experiments and modeling. *Acta Mater.* **2021**, *220*, 117338. [[CrossRef](#)]
5. Franco-Correa, J.C.; Martínez-Franco, E.; Alvarado-Orozco, J.M.; Cáceres-Díaz, L.A.; Espinosa-Arbelaez, D.G.; Villada, J.A. Effect of Conventional Heat Treatments on the Microstructure and Microhardness of IN718 Obtained by Wrought and Additive Manufacturing. *J. Mater. Eng. Perform.* **2021**, *30*, 7035. [[CrossRef](#)]
6. Chamanfar, A.; Sarrat, L.; Jahazi, M.; Asadi, M.; Weck, A.; Koul, A.K. Microstructural characteristics of forged and heat treated Inconel-718 disks. *Mater. Design* **2013**, *52*, 791–800. [[CrossRef](#)]
7. He, D.; Lin, Y.C.; Tang, Y.; Li, L.; Chen, J.; Chen, M.; Chen, X. Influences of solution cooling on microstructures, mechanical properties and hot corrosion resistance of a nickel-based superalloy. *Mater. Sci. Eng. A* **2019**, *746*, 372–383. [[CrossRef](#)]
8. Firoz, R.; Basantia, S.K.; Khutia, N.; Bar, H.N.; Sivaprasad, S.; Murthy, G.V.S. Effect of microstructural constituents on mechanical properties and fracture toughness of Inconel 718 with anomalous deformation behavior at 650 °C. *J. Alloys Compd.* **2020**, *845*, 156276. [[CrossRef](#)]
9. Chen, Y.; Yeh, A.; Li, M.; Kuo, S. Effects of processing routes on room temperature tensile strength and elongation for Inconel 718. *Mater. Design* **2017**, *119*, 235–243. [[CrossRef](#)]
10. Rafiei, M.; Mirzadeh, H.; Malekan, M. Precipitation kinetics of γ'' phase and its mechanism in a Nb-bearing nickel-based superalloy during aging. *Vacuum* **2020**, *178*, 109456. [[CrossRef](#)]

11. Drexler, A.; Oberwinkler, B.; Primig, S.; Turk, C.; Povoden-Karadeniz, E.; Heinemann, A.; Ecker, W.; Stockinger, M. Experimental and numerical investigations of the γ'' and γ' precipitation kinetics in Alloy 718. *Mater. Sci. Eng. A* **2018**, *723*, 314–323. [[CrossRef](#)]
12. Fisk, M.; Andersson, J.; du Rietz, R.; Haas, S.; Hall, S. Precipitate evolution in the early stages of ageing in Inconel 718 investigated using small-angle x-ray scattering. *Mater. Sci. Eng. A* **2014**, *612*, 202–207. [[CrossRef](#)]
13. Qin, H.; Bi, Z.; Yu, H.; Feng, G.; Zhang, R.; Guo, X.; Chi, H.; Du, J.; Zhang, J. Assessment of the stress-oriented precipitation hardening designed by interior residual stress during ageing in IN718 superalloy. *Mater. Sci. Eng. A* **2018**, *728*, 183–195. [[CrossRef](#)]
14. Ran, Q.; Xiang, S.; Tan, Y. Improving Mechanical Properties of GH4169 Alloys by Reversing the Deformation and Aging Sequence. *Adv. Eng. Mater.* **2021**, *23*, 2100386. [[CrossRef](#)]
15. Ye, N.; Cheng, M.; Zhang, S.; Song, H.; Zhou, H.; Wang, P. Effect of δ Phase on Mechanical Properties of GH4169 Alloy at Room Temperature. *J. Iron Steel Res. Int.* **2015**, *22*, 752–756. [[CrossRef](#)]
16. Deng, H.; Wang, L.; Liu, Y.; Song, X.; Meng, F.; Yu, T. Microstructure and tensile properties of IN718 superalloy aged with temperature/stress coupled field. *J. Mater. Res. Technol.* **2023**, *23*, 4747–4756. [[CrossRef](#)]
17. Ramalho Medeiros, M.A.; de Melo, C.H.; Pinto, A.L.; de Almeida, L.H.; Araújo, L.S. The δ phase precipitation during processing and the influence on grain boundary character distribution and mechanical properties of superalloy 718. *Mater. Sci. Eng. A* **2018**, *726*, 187–193. [[CrossRef](#)]
18. Roth, H.A.; Davis, C.L.; Thomson, R.C. Modeling solid solution strengthening in nickel alloys. *Metall. Mater. Trans. A* **1997**, *28*, 1329. [[CrossRef](#)]
19. Sui, S.; Tan, H.; Chen, J.; Zhong, C.; Li, Z.; Fan, W.; Gasser, A.; Huang, W. The influence of Laves phases on the room temperature tensile properties of Inconel 718 fabricated by powder feeding laser additive manufacturing. *Acta Mater.* **2019**, *164*, 413–427. [[CrossRef](#)]
20. Zhang, Y.; Lan, L.; Zhao, Y. Effect of precipitated phases on the mechanical properties and fracture mechanisms of Inconel 718 alloy. *Mater. Sci. Eng. A* **2023**, *864*, 144598. [[CrossRef](#)]
21. Slama, C.; Servant, C.; Cizeron, G. Aging of the Inconel 718 alloy between 500 and 750 °C. *J. Mater. Res.* **1997**, *12*, 2298–2316. [[CrossRef](#)]
22. Devaux, A.; Nazé, L.; Molins, R.; Pineau, A.; Organista, A.; Guédou, J.Y.; Uginet, J.F.; Héritier, P. Gamma double prime precipitation kinetic in Alloy 718. *Mater. Sci. Eng. A* **2008**, *486*, 117–122. [[CrossRef](#)]
23. Sundararaman, M.; Mukhopadhyay, P.; Banerjee, S. Some aspects of the precipitation of metastable intermetallic phases in INCONEL 718. *Metall. Trans. A* **1992**, *23*, 2015–2028. [[CrossRef](#)]
24. Lu, X.D.; Du, J.H.; Deng, Q. High temperature structure stability of GH4169 superalloy. *Mater. Sci. Eng. A* **2013**, *559*, 623–628. [[CrossRef](#)]
25. Qin, H.; Bi, Z.; Yu, H.; Feng, G.; Du, J.; Zhang, J. Influence of stress on γ'' precipitation behavior in Inconel 718 during aging. *J. Alloys Compd.* **2018**, *740*, 997–1006. [[CrossRef](#)]
26. Oblak, J.M.; Duvall, D.S.; Pauloni, D.F. An estimate of the strengthening arising from coherent, tetragonally-distorted particle. *Mater. Sci. Eng.* **1974**, *13*, 51–56. [[CrossRef](#)]
27. He, D.G.; Lin, Y.C.; Jiang, X.Y.; Yin, L.X.; Wang, L.H.; Wu, Q. Dissolution mechanisms and kinetics of δ phase in an aged Ni-based superalloy in hot deformation process. *Mater. Design* **2018**, *156*, 262–271. [[CrossRef](#)]
28. Anderson, M.; Thielin, A.L.; Bridier, F.; Bocher, P.; Savoie, J. δ Phase precipitation in Inconel 718 and associated mechanical properties. *Mater. Sci. Eng. A* **2017**, *679*, 48–55. [[CrossRef](#)]
29. Cai, D.; Zhang, W.; Nie, P.; Liu, W.; Yao, M. Dissolution kinetics of δ phase and its influence on the notch sensitivity of Inconel 718. *Mater. Charact.* **2007**, *58*, 220–225. [[CrossRef](#)]
30. Lian, X.T.; An, J.L.; Wang, L.; Dong, H. A New Strategy for Restraining Dynamic Strain Aging in GH4169 Alloy During Tensile Deformation at High Temperature. *Acta Metall. Sin.* **2022**, *35*, 1895–1902. [[CrossRef](#)]
31. Zhao, J.; Hung, F.; Lui, T. Microstructure and tensile fracture behavior of three-stage heat treated inconel 718 alloy produced via laser powder bed fusion process. *J. Mater. Res. Technol.* **2020**, *9*, 3357–3367. [[CrossRef](#)]
32. Cui, C.; Zhang, R.; Zhou, Y.; Sun, X. Portevin-Le Châtelier effect in wrought Ni-based superalloys: Experiments and mechanisms. *J. Mater. Sci. Technol.* **2020**, *51*, 16–31. [[CrossRef](#)]

Disclaimer/Publisher's Note: The statements, opinions and data contained in all publications are solely those of the individual author(s) and contributor(s) and not of MDPI and/or the editor(s). MDPI and/or the editor(s) disclaim responsibility for any injury to people or property resulting from any ideas, methods, instructions or products referred to in the content.